Alignment of particles in sheared viscoelastic fluids

Alignment of particles in sheared viscoelastic fluids

I. S. Santos de Oliveira, A. van den Noort, J. T. Padding, W. K. den Otter, and W. J. Briels

Citation: J. Chem. Phys. **135**, 104902 (2011); doi: 10.1063/1.3633701
View online: http://dx.doi.org/10.1063/1.3633701
View Table of Contents: http://jcp.aip.org/resource/1/JCPSA6/v135/i10
Published by the American Institute of Physics.

Alignment of particles in sheared viscoelastic fluids

I. S. Santos de Oliveira,[1,a)] A. van den Noort,[1] J. T. Padding,[1,2]
W. K. den Otter,[1] and W. J. Briels[1,b)]
[1]*Computational Biophysics, University of Twente, P.O. Box 217, 7500 AE, Enschede, The Netherlands*
[2]*Institut de la Matière Condensée et des Nanosciences, Université Catholique de Louvain, Croix du Sud 1, 1348 Louvain-la-Neuve, Belgium*

(Received 20 June 2011; accepted 15 August 2011; published online 14 September 2011)

We investigate the shear-induced structure formation of colloidal particles dissolved in non-Newtonian fluids by means of computer simulations. The two investigated visco-elastic fluids are a semi-dilute polymer solution and a worm-like micellar solution. Both shear-thinning fluids contain long flexible chains whose entanglements appear and disappear continually as a result of Brownian motion and the applied shear flow. To reach sufficiently large time and length scales in three-dimensional simulations with up to 96 spherical colloids, we employ the responsive particle dynamics simulation method of modeling each chain as a single soft Brownian particle with slowly evolving inter-particle degrees of freedom accounting for the entanglements. Parameters in the model are chosen such that the simulated rheological properties of the fluids, i.e., the storage and loss moduli and the shear viscosities, are in reasonable agreement with experimental values. Spherical colloids dispersed in both quiescent fluids mix homogeneously. Under shear flow, however, the colloids in the micellar solution align to form strings in the flow direction, whereas the colloids in the polymer solution remain randomly distributed. These observations agree with recent experimental studies of colloids in the bulk of these two liquids. © *2011 American Institute of Physics*. [doi:10.1063/1.3633701]

I. INTRODUCTION

The response of a Newtonian liquid to shear deformation is to develop a stress proportional to the applied shear rate. Non-Newtonian fluids, in contrast, display a variety of more complex stress versus rate-of-strain relationships. For example, they can have elastic properties, have long-lived memories of earlier states, or have an apparent viscosity that depends on how fast you shear them. Such fluids have many practical uses, e.g., as industrial lubricants, as drilling and fracturing fluids that improve oil recovery from oil wells, and as thickeners in the paint and food industry.[1] Non-Newtonian fluids are also important in biology: a well-known non-Newtonian fluid is blood. In this paper we present simulations of shear-thinning liquids, i.e., fluids whose apparent viscosities decrease with increasing shear rate, and study the ordering of dispersed solid particles in these fluids under shear.

Colloidal particles in sheared viscoelastic fluids are frequently observed to spontaneously form colloidal chains along the flow direction, depending on the fluid's flow characteristics, applied shear rate and boundary conditions, while this behavior is not observed in simple Newtonian fluids. This poorly understood phenomenon was already reported in 1977 by Michele *et al.*[2] and confirmed a decade ago by Lyon *et al.*[3] In these studies it was suggested that colloidal alignment appears when the Weissenberg number, defined as the ratio of first normal stress difference to shear stress, is larger than 10. Subsequent work by Scirocco *et al.*[4] and Won and Kim[5] showed that this critical Weissenberg number is not universal. These studies also established that viscoelasticity is not a sufficient condition for structure formation, since alignment is not observed in viscoelastic Boger fluids.[4,5] Instead, these authors suggested that shear-thinning is a necessary condition for shear-induced alignment of spherical particles. The recent work of Pasquino *et al.*[6] on dilute suspensions of hard spheres in a worm-like micellar solution showed the formation of string-like structures at low shear rates and 2D crystals at high shear rates. For a review on flow-induced ordering in complex fluids, we refer the reader to Malkin *et al.*[7] The Vermant group[8] has recently shown that alignment typically occurs at the walls of the rheometer, following colloidal migration from the bulk towards these walls. Worm-like micellar solutions are exceptional by producing alignment in the bulk. Here, our focus will be on (dis)ordering of colloids in bulk viscoelastic fluids.

There is much practical interest in gaining control over the arrangement of particles embedded in fluids. For example, Manski *et al.*[9] suggested that controlled structuring is very useful in food engineering. It is, therefore, important to gain more insight into the still poorly understood process of colloidal structuring under flow. Here, we show how advances in computer simulation methods offer new possibilities to obtain such insights. The problem of simulating colloids dispersed in viscoelastic fluids has been considered before by a number of groups, using lattice methods and Stokesian approaches to calculate flow fields subject to the boundary conditions posed by the colloids. Feng *et al.*,[10] Binous and Phillips,[11] Harlen,[12] Yu *et al.*,[13] and Ardekani *et al.*[14] simulated one and two spheres sedimenting through a viscoelastic fluid. Hwang *et al.*[15] studied kissing and tumbling of two colloids in shear flow and observed strong shear-induced elongational flows

a)Electronic mail: i.s.santosdeoliveira@utwente.nl.
b)Electronic mail: w.j.briels@utwente.nl.

between six colloids. Patankar and Hu[16] simulated the migration of a colloid towards the centerline of a channel in a pressure-driven flow. D'Avino *et al.*[17–19] analyzed the rotation of a particle in a sheared viscoelastic liquid, and the shear-induced migration of a particle towards a wall. Flow-induced aggregation of a dozen colloids in a viscoelastic solution was simulated by Yu *et al.*[13] for sedimenting particles and by Phillips and Talini[20] and Hwang and Hulsen[21] for suspensions exposed to a shear flow. We note that these studies have in common that the three-dimensional calculations have been limited to one and two colloidal particles in a viscoelastic fluid, while simulations with up to a dozen colloids were all restricted to two dimensions.

In this paper, we show that the particle-based off-lattice responsive particle dynamics (RaPiD) method[22,23] efficiently simulates various viscoelastic fluids, is easily applied to fluids containing many colloids, and thereby makes possible the computational study in three dimensions of colloidal ordering under shear flow. To study the effect of the viscoelastic fluid on the alignment in the bulk, we study three-dimensional dispersions of up to 96 spherical colloids in two distinct shear-thinning viscoelastic solutions. One fluid models a solution of polyisobutylene (PIB) dissolved in pristane, with polymers of molecular weight $M_w = 1.2 \times 10^3$ kg/mol. The second fluid models a worm-like micellar solution of cetylpyridiniumchloride (CPyCl) and sodiumsalicylate (NaSal) in salt water, at concentrations of 100 mM and 60 mM, respectively. In Section II, we describe how these fluids are simulated using the RaPiD method. In Section III, we show that the RaPiD model is able to reproduce the experimental bulk rheological properties of both fluids[24] reasonably well. Spherical particles are immersed in these fluids in Section IV, and the dispersions are next subjected to shear flow to study the resulting ordering, or lack of ordering, of the colloids. The main conclusions are summarized in Section V.

II. SIMULATION METHOD

A. Background

To reach the large time and length scales required in simulations of colloidal ordering, we will coarse-grain entire polymer chains and worm-like micelles to single particles. Each polymer and micelle is represented by just the position of its center-of-mass. This is not to say that all the removed coordinates are irrelevant for the rheology of the system. On the one hand, the eliminated coordinates provide the free energy function Φ_C, the so-called potential of mean force, which governs the equilibrium distribution of the N_p centers of mass. In thermodynamic equilibrium, the probability distribution $P_{\text{eq}}(r)$ of the center-of-mass positions r is given by

$$P_{\text{eq}}(r) \propto \exp\left[-\beta \Phi_C(r)\right], \tag{1}$$

where $\beta = 1/k_B T$ is the inverse of the thermal energy, with Boltzmann's constant k_B and temperature T. On the other hand, the removed coordinates give rise to friction and random forces in the equations of motion for the retained coordinates.[25,26] In most coarse-grain representations of soft matter systems, these frictions and random forces necessarily have "memory" of the configurations the system has gone through in the recent, and sometimes even the distant past.[23] For example, when describing polymeric systems on the level of their centers of mass, as we do here, the friction and random forces must effectively represent all important effects caused by the entanglements; a simple Brownian dynamics propagator with realistic mean forces and Markovian random displacements will not reproduce representative paths of the retained coordinates. To circumvent the introduction of memory effects in the friction forces and stochastic displacements, we employ the RaPiD method.[22,23]

The idea behind the RaPiD method is to introduce a relatively small set of additional dynamic variables which keep track, in a coarse-grained manner, of the thermodynamic state of the eliminated coordinates. Deviations of these additional variables from their equilibrium values, with the latter being determined by the configuration r of the retained coordinates, give rise to additional forces acting on the retained coordinates, on top of the thermodynamic forces derived from the potential of mean force. In the RaPiD method, these additional non-equilibrium forces are specifically designed with the propensity to resist deformation of the configuration r, by driving the system back to its earlier state, while at the same time these forces slowly fade away as the additional variables relax toward their new equilibrium values for the new configuration. This particular combination of characteristics, i.e., the transient resistance to deformation, endows the simulated fluid with a viscoelastic behavior. In the current study of semi-dilute polymer and worm-like micellar solutions at nearly 15 times the critical overlap concentration, the dominant physical mechanism giving rise to viscoelastic behavior is the entanglement of the chains; the additional transient forces will therefore also be referred to as the entanglement forces. The versatility of the RaPiD method is illustrated by successful applications to fluids as diverse as solutions of polymeric core-shell colloids,[27] highly entangled polymer melts,[28] telechelic polymer networks,[29] solutions of star polymers,[30] and glue,[31] and its ability to simulate flow phenomena ranging from shear thinning,[22] shear banding[27] and shear fracture[32] to microscopic phase separation and lamellar re-orientation under shear.[33]

B. Conservative forces

The configurational free energy Φ_C of a semi-dilute solution of polymeric or worm-like micellar chains is conveniently described by the Flory-Huggins (FH) theory.[34,35] We adapt the FH model here, following Kindt and Briels,[28] to calculate the local free energy subject to the given center-of-mass positions of the chains; this free energy takes into account all possible configurations of the monomers in the chains and of the solvent. It will be assumed that this local free energy can be expressed as a function of the local number density of polymers. During the simulation, the local number density around a specific polymer i is calculated as

$$\rho_i = \sum_{j=1}^{N_p} \omega(r_{ij}), \tag{2}$$

where N_p is the number of chains (polymers or worms) in the system and $\omega(r)$ is a suitably normalized weight function. There is no rigorous way to define this weight function, but some demands should be satisfied. The weight as a function of the distance to the chain's center will be a monotonously decreasing function. The weight function must have a non-zero derivative at the origin, otherwise the vanishing repulsive forces at very short distances do not prevent the formation of clusters. To avoid discontinuities in the force at the cut-off radius r_c, the weight function and its first derivative should go to zero smoothly. We use simple linear and quadratic expressions to satisfy these demands,

$$\omega(r_{ij}) = \begin{cases} c(r_c - r_s)(r_c + r_s - 2r_{ij}) & ; \quad r_{ij} \leq r_s \\ c(r_{ij} - r_c)^2 & ; \; r_s < r_{ij} \leq r_c \\ 0 & ; \; r_c < r_{ij}, \end{cases} \tag{3}$$

where r_s denotes the distance where the weight function switches from linear to quadratic, and c is a normalization constant chosen such that $\int \omega(r_{ij}) \mathrm{d}\mathbf{r} = 1$. Because the range of chain-chain interactions is of the order of the chain radius of gyration R_g, we choose $r_c = 2.5R_g$ and $r_s = R_g$. We note that there is no conservation law associated with the local densities ρ_i, i.e., $\langle \rho_i \rangle \neq \rho$ in general, where $\rho = N_p/V$ is the box-averaged number density. Nevertheless, ρ_i provides a reasonable measure for the local polymer number density at the position of polymer i.

The local polymer volume fraction ϕ_i entering the Flory-Huggins free energy expression may now be defined as

$$\phi_i = \frac{\rho_i}{\rho_{\max}}, \tag{4}$$

where $\rho_{\max}$ defines the maximum local polymer density, i.e., the density of a solvent-free polymer melt and, therefore, $\phi_i \leq 1$. Using the procedure described in the Appendix, we can approximate the total free energy of the system, for a given configuration r, as a sum of particle contributions,

$$\Phi_C = \sum_{i=1}^{N_p} a^p(\phi_i), \tag{5}$$

where the free energy per chain $a^p(\phi_i)$, as a function of the local chain density, reads as

$$a^p(\phi_i) = pk_BT \left\{ \frac{1-\phi_i}{\phi_i} \ln(1-\phi_i) - \chi\phi_i \right\}. \tag{6}$$

Here p is the number of Kuhn segments in the chain and χ is the usual Flory-Huggins parameter as defined in Eq. (A5). The resulting thermodynamic forces acting on the particles are readily derived by differentiating Eq. (5), as is shown in the Appendix. We note that the denominator to the fraction in Eq. (6) will never be zero, by virtue of the self-term in Eq. (2); besides this, the limit of $a^p(\phi_i)$ when ϕ_i approaches zero is constant.

C. Transient forces

We now turn our attention to the transient forces, which were already qualitatively introduced at the start of this section. The motion of a chain in a polymer solution (or in a worm-like micellar solution) is slowed down predominantly by entanglements with neighboring chains. The corresponding transient forces are approximately included in the RaPiD method by introducing an additional variable n_{ij} for every close pair of chains i and j. This additional variable will be referred to as the number of entanglements that exist between this pair of chains, but we note that any type of chain intermixing that slows down the dynamics is included. The entanglement force between particles i and j will be assumed linear in the deviation of the entanglement number from the equilibrium number of entanglements $n_0(r_{ij})$ for the given distance between the two particles. The "entanglement potential" behind the entanglement force is then given by

$$\Phi_t(r, n) = \frac{1}{2}\alpha \sum_{i,j} (n_{ij} - n_0(r_{ij}))^2, \tag{7}$$

where α determines the variance of the fluctuations in n_{ij} and the sum runs over all neighboring particle pairs. The equilibrium entanglement number $n_0(r_{ij})$ depends on the probability of having monomers of the two chains in close proximity, i.e., n_0 is proportional to the overlap of two chains. For Gaussian chains, the distribution of monomers around the center of mass of a chain is approximately a Gaussian distribution[36] and the overlap is again an approximately Gaussian function of the separation between the centers of mass.[37] However, to avoid zero forces at short distances, we choose to represent $n_0(r_{ij})$ not by a Gaussian but by a good fitting quadratic function that, furthermore, smoothly vanishes at the cut-off radius,

$$n_0(r_{ij}) = \begin{cases} \left(\frac{r_{ij}}{r_c} - 1 \right)^2 & ; \quad r_{ij} \leq r_c \\ 0 & ; \; r_{ij} > r_c. \end{cases} \tag{8}$$

Because n_{ij} and $n_0(r)$ always appear in combination with α in the entanglement force and potential, we are free to choose a suitable normalization for n_0, and hence n_{ij}, while retaining α as a fit parameter of the model. We have chosen $n_0 = 1$ at $r = 0$, and consequently $n_0(r)$ may loosely be interpreted as the *fraction* of maximum overlap.

Given the conservative and entanglement potentials, the equilibrium probability density Ψ to encounter a certain configuration r in combination with a set of entanglement numbers n reads as

$$\Psi(r, n) \propto \exp\{-\beta[\Phi_C(r) + \Phi_t(r, n)]\}. \tag{9}$$

One readily shows that integration over n, exploiting the quadratic structure of Φ_t, recovers the equilibrium probability density of Eq. (1). We, therefore, conclude that the entanglement forces alter the dynamical properties of a fluid but not its thermodynamical properties. This property will be used below to show that variations in the dynamical properties alone suffice to generate markedly different alignment behavior.

D. Equations of motion

Having defined the potential, the displacement of particle i over a simulation time step dt on the Smoluchowski time

scale is given by[22,23]

$$d\mathbf{r}_i = -\frac{1}{\xi_i}\left(\nabla_i \Phi_C + \nabla_i \Phi_t\right) dt + \nabla_i \left(\frac{k_B T}{\xi_i}\right) dt + \Theta_i \sqrt{\frac{2k_B T dt}{\xi_i}}. \quad (10)$$

The first term on the right-hand side is the contribution of conservative and entanglement forces, with the particle-dependent friction parameter ξ_i to be discussed below. The middle term corrects for a spurious drift that would otherwise have resulted in a finite time step algorithm from the non-constancy of the friction coefficient. The last term describes Brownian displacements of the particles, where the components of the time-dependent Markovian random vector Θ_i have unit variance and zero mean, the three Cartesian components are independent and the set of vectors is devoid of inter-particle correlations. Since the friction experienced by a chain is mainly due to entanglements, we assume that the friction coefficient of particle i is proportional to the actual number of entanglements of particle i with its neighbors,

$$\xi_i = \xi_0 + \xi_e \sum_{j \neq i} \sqrt{n_{ij} n_0(r_{ij})}, \quad (11)$$

where ξ_e is the friction per entanglement and ξ_0 is the background friction by the solvent. By taking the geometric average of n_{ij} with the equilibrium number of entanglements $n_0(r_{ij})$, we ensure that the entanglement friction between particles smoothly ceases at the cut-off distance r_c.

The equation of motion for the entanglement number n_{ij}, again on the Smoluchowski time scale, is given by[22,23]

$$dn_{ij} = \frac{1}{\tau}(n_0(r_{ij}) - n_{ij})dt + \Theta_{ij}\sqrt{\frac{2k_B T dt}{\alpha \tau}}. \quad (12)$$

In the last term on the right-hand side, Θ_{ij} is a time-dependent random Markovian scalar with zero mean, unit average, and without correlation across particle pairs. For convenient interpretation, the friction coefficient slowing down the entanglement dynamics has been expressed here as $\alpha\tau$, where τ denotes the characteristic relaxation time. We expect the collective entanglements between two chains in close proximity to be of a more severely interwoven nature than those between two distant weakly entwined chains, and therefore the former will take longer to relax than the latter. To take this effect into account, we let the relaxation time depend on the distance between the particles,

$$\tau_{ij} = \tau_0 \exp\left(-\frac{r_{ij}}{\lambda}\right), \quad (13)$$

where τ_0 is a time constant and λ denotes the decay length of the relaxation time.

All simulations are performed in rectangular boxes of fixed dimensions, using periodic boundary conditions.[38] In a large number of simulations, a shear flow is applied along the x-direction, with a velocity gradient $\dot{\gamma}$ in the y-direction, by using Lees-Edwards sliding boundary conditions[38] in combination with a slightly modified equation of motion. Every time step, the instantaneous flow field in the x-direction is determined for a set of planes at equally spaced heights along the y axis, by attributing the displacements of each particle to its two surrounding planes by a lever-rule. This noisy flow field is then smoothed by averaging over the flow field history, at every height, using an exponentially decaying weight function with a decay time $\tau_{\text{flow}} = 10^{-3}$ s, to obtain the fluid velocity function $V(y)$. By re-deriving the equations of motion, with particle i now experiencing a friction relative to the flow field at height y_i, the displacement in Eq. (10) acquires the additional term $+V(y_i)\hat{\mathbf{e}}_x dt$. This approach has been applied successfully in the earlier RaPiD simulations, see, e.g., Refs. 29, 39, and 40. and proved sufficiently flexible to permit shear banding and shear fracture. We emphasize the absence of walls in these simulations, which consequently faithfully reproduce bulk shear flow.

III. TWO SHEAR-THINNING FLUIDS

A. Model parameters

The above described RaPiD method was applied to simulate two distinct shear-thinning viscoelastic fluids. As the first fluid, we studied a polymer solution of a high molecular weight PIB ($M_w = 1.2 \times 10^3$ kg/mol) dissolved in pristane; this mixture, and behavior of colloids dispersed in this fluid, was the subject of recent experiments by Snijkers *et al.*[24] These experimental data guided the parameterization of the simulation model, as summarized in Table I. The table is divided in the "set parameters," listing experimentally known quantities, and the "simulation parameters," the fitting parameters established to reproduce the experimental rheology of the fluid. In particular, we tuned α, ξ_e, τ_0, and λ for agreement with the experimental zero shear viscosity η_0 and the storage and loss moduli $G'(\omega)$ and $G''(\omega)$, which will be discussed in Section III C.

As the second fluid, we studied a worm-like micellar solution modeled after an experimental mixture of 100 mM CPyCl and 60 mM NaSal in salt water. To parameterize the fluid, we took the polymer solution as a reference and adjusted only the parameters related to the entanglement forces. That is, we combined the set parameters of the polymer solution with the new values for α, ξ_e, τ_0, and λ listed at the bottom of Table I. Since the two fluids are microscopically very different, it may come at first sight as a surprise that the potential of mean force Φ_C of the polymer solution has been used to represent a worm-like micellar solution. It should be realized, however, that both polymers and worm-like micelles form long and flexible chains, which reduces the effective interaction between their centers of mass of the chains to a very soft repulsive potential. Therefore, the conservative interactions between polymers and micellar worms are quite similar, and both are relatively unimportant to the flow behavior, which will be dominated by entanglements. Moreover, we are mainly interested in the rheological effects of each fluid, and a clearer comparison will be possible if the equilibrium structures of the two fluids are assumed to be the same.

The transient force parameters of the worm-like solution, like those of the polymer solution discussed before, were tuned such that good agreement is obtained with the experimental zero-shear viscosity η_0 and the storage and loss

TABLE I. The simulation parameters of the polymer solution and the worm-like micellar solution.

Set parameters	
Temperature	$T = 300\text{K}$
Radius of gyration	$R_g = 40\text{nm}$
Density	$\rho_p = 3.5\,\text{pol}/R_g^3$
Average volume fraction	$\phi = 0.11 \rightarrow \rho_{\max}/\overline{\rho} = 9$
Flory-Huggins parameter	$\chi = 0.5$
Number of monomers	$p = 2700\,\text{mon.}/\text{polymer}$
Solvent viscosity	$\eta_s = 5 \times 10^{-3}\,\text{Pa s}$
Solvent friction	$\xi_0 = 2.45 \times 10^{-9}\,\text{kg/s}$
Polymer solution simulation parameters	
Cut-off range	$r_c = 2.5\,R_g$
Density critical radius	$r_s = 1.0\,R_g$
Entanglement number deviation	$\alpha = 10\,k_BT$
Entanglement friction	$\xi_e = 5 \times 10^{-9}\,\text{kg/s}$
Maximum entanglement relaxation time	$\tau_0 = 250\,\text{s}$
Decay length of entanglement relaxation time	$\lambda = 0.2\,R_g$
Wormlike micellar solution simulation parameters	
Cut-off range	$r_c = 2.5\,R_g$
Density critical radius	$r_s = 1.0\,R_g$
Entanglement number deviation	$\alpha = 0.1\,k_BT$
Entanglement friction	$\xi_e = 7 \cdot 10^{-7}\text{kg/s}$
Maximum entanglement relaxation time	$\tau_0 = 200\,\text{s}$
Decay length of entanglement relaxation time	$\lambda = \infty$

moduli $G'(\omega)$ and $G''(\omega)$, which will be discussed in Section III C. The resulting changes, compared to the polymer solution, are a much smaller entanglement strength α and a much larger entanglement friction ξ_e. Also, the entanglement relaxation time τ is now truly constant, i.e., $\tau = \tau_0$ for $\lambda \rightarrow \infty$, in agreement with the observation that a well-entangled worm-like micellar solution effectively has a single relaxation time.[41–44]

B. Structural properties

The simulations with quiescent fluids were carried out for cubic boxes containing 804 particles in a volume $V = 230R_g^3$. To analyze the structural properties of the system, we calculated the radial distribution function $g(r)$ and the structure factors $S(k)$. Looking at Fig. 1, we observe the absence of any clear structure in the system, and only a small correlation hole occurs below distances of the order of R_g. The non-zero $g(r)$ for small distances indicates that the particles can approach each other very closely, which reflects the ability of long flexible chains to coalesce their centers of mass without generating any overlap at the monomeric scale. The structure factors $S(k)$, shown in the inset to Fig. 1, confirm the absence of structure in the polymer center of mass distribution. These structural results are in agreement with atomistic Monte Carlo simulations of long linear polymers, e.g., polyethylene.[45]

Since we used the same conservative potential for both polymer and worm-like micelles solutions, their equilibrium results should be the same. Our results confirmed that they are very similar indeed, and thereby support the comment below

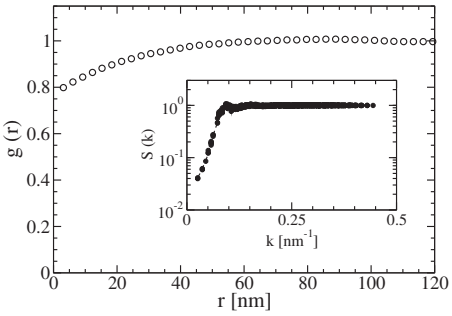

FIG. 1. Radial distribution function (main plot) and structure factor (inset) for the polymer solution. The nearly structureless distribution, with a slight correlation hole below $R_g = 40$ nm, is typical for the center of mass distribution of long flexible chains. The solution of worm-like micelles yielded identical curves, as it is based on the same conservative interactions.

Eq. (9) that the transient forces do not perturb the equilibrium structure of the systems.

C. Dynamic properties

The linear rheology of the model fluids was obtained from equilibrium simulations by computing the autocorrelation of the shear stress. The relevant component of the shear stress tensor is given by

$$S_{xy}(t) = -\frac{1}{V}\sum_{i,j}(r_{i,x} - r_{j,x})F_{ij,y}, \tag{14}$$

with $F_{ij,y}$ denoting the y-component of the force on particle i due to conservative and entanglement interactions with particle j. The autocorrelation of the shear stress yields the shear relaxation modulus,

$$G(t) = \frac{V}{k_BT}\langle S_{xy}(t)S_{xy}(0)\rangle. \tag{15}$$

Integration of $G(t)$ from $t = 0$ to ∞ results in the zero-shear viscosity η_0, while the real and imaginary parts of its Fourier transform yield the storage modulus G' and loss modulus G'',

$$G'(\omega) = \omega\int_0^\infty \sin(\omega t)G(t)\mathrm{d}t, \tag{16}$$

$$G''(\omega) = \omega\int_0^\infty \cos(\omega t)G(t)\mathrm{d}t, \tag{17}$$

respectively.

The shear-thinning behavior of both fluids was analyzed by applying shear flow. From the steady-state shear stresses over a wide range of shear rates, the apparent viscosity was calculated as

$$\eta(\dot\gamma) = \frac{S_{xy}(\dot\gamma)}{\dot\gamma}. \tag{18}$$

The simulation results are discussed next.

The integral of $G(t)$ of the polymer solution yielded a zero-shear viscosity $\eta_0 = 70$ Pa s, in close agreement with the experimental value of 75 Pa s.[24] Figure 2 shows that the storage and loss moduli agree qualitatively with their experimental counterparts, and match the experimental crossover angular frequency of 20 rad/s. We did not tune the parameters of the model any further to get better agreement with

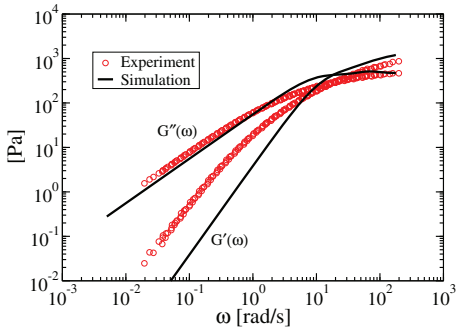

FIG. 2. Storage modulus $G'(\omega)$ and loss modulus $G''(\omega)$ of the polymer solution over a range of frequencies. The black solid lines are simulation results, obtained as Fourier transforms of $G(t)$, and the red circles denote experimental results by Snijkers *et al.* (Ref. 24).

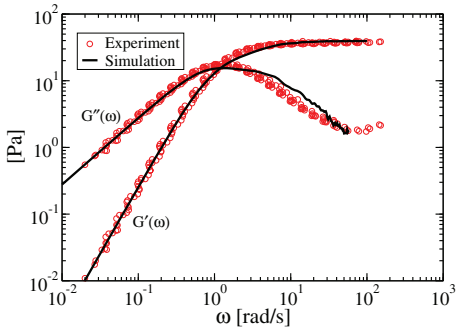

FIG. 4. Storage modulus $G'(\omega)$ and loss modulus $G''(\omega)$ of the worm-like micellar solution, with the black solid lines showing simulation results and the red circles denoting experimental results by Snijkers *et al.* (Ref. 24).

experiments since our goal in this paper is to provide a proof of principles only. Moreover, the experimental system was polydisperse, asking for much more elaborate simulations. The shear viscosity extracted from simulations under shear, see Fig. 3, is fairly constant for low shear rates up to 1 s^{-1}, as is the experimental shear viscosity. At high shear rates the viscosity shows a steady decline—the main characteristic of a shear-thinning fluid—with the viscosity of the model fluid decaying slightly steeper than that of the real fluid. We did not observe shear-banding in the applied range of shear rates.

Equilibrium simulations of the worm-like micellar solution yielded a zero-shear viscosity of 28 Pa s, in excellent agreement with the experimental value of 28 Pa s.[24] The storage and loss moduli, plotted in Fig. 4, closely follow their experimental counterparts. The rheological behavior of this system is well captured by a Maxwell model, as was also reported by Refs. 1 and 44, while the polymer solution shows the hallmarks of a fluid with a distribution of relaxation times. Simulations of sheared solutions yielded the shear viscosity curve of Fig. 5. The plateau at low shear rates and the rate of decline at high shear rates are in quantitative agreement with experimental data, though the onset of shear-thinning occurs at a slightly lower shear rate in the simulations. Despite a shear-thinning exponent of nearly −1, we did not observe shear-banding for the shear rates used here.

IV. COLLOIDAL DISPERSIONS

A. Spherical colloids

The viscoelastic fluids of Sec. III were used to suspend spherical colloids, with colloidal radii equal to the radius of gyration of the polymer and micellar chains, $R_{\rm col} = R_g = 40$ nm. These colloids are much smaller than the colloids used in the recent experiments with dispersions in the same fluids by Pasquino *et al.*,[6] since the experimental radius would have led to prohibitively large simulation boxes. Because of the smaller size, Brownian displacements play a more important role in the simulations than in the experiments. At a typical shear rate of 15 s^{-1}, corresponding to Deborah numbers of $De = \dot\gamma\tau_{\rm cross} = 0.8$ and 12 for the polymer and micellar solutions, respectively, the Peclet numbers are $Pe = 6\pi R_{\rm col}^3\dot\gamma\eta(\dot\gamma)/k_BT = 86$ and 3, respectively. While the stronger thermal fluctuations may affect the relaxation process of the sheared colloidal fluids, we do not expect the Brownian motion to significantly alter the steady state. From the below descriptions of the simulations, it indeed emerges that the smaller colloidal size is of little consequence to the shear-alignment of the colloids.

The colloid-colloid and colloid-polymer interaction potentials are plotted in Fig. 6 against their respective distances. For colloid-colloid interactions we choose a relatively hard potential, scaling as D_S^{-8} with the surface-to-surface distance $D_S = r - 2R_{\rm col}$ between a pair of colloids. The

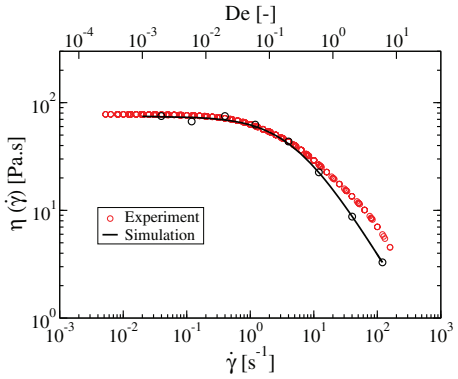

FIG. 3. The apparent shear viscosity of the polymer solution as a function of applied shear rate, and of Deborah number ($De = \dot\gamma\tau_{\rm cross}$), showing in black our simulation results and in red the experimental results by Snijkers *et al.* (Ref. 24).

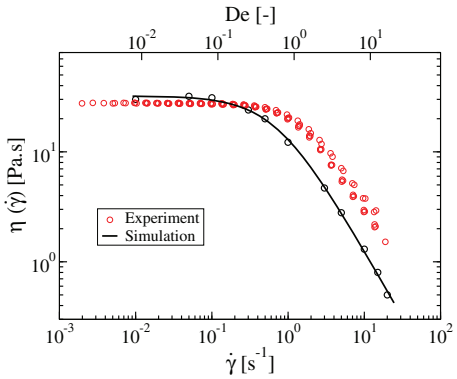

FIG. 5. Shear viscosity curve for the worm-like micellar solution, showing simulation results (black) and experimental results (red) by Snijkers *et al.* (Ref. 24).

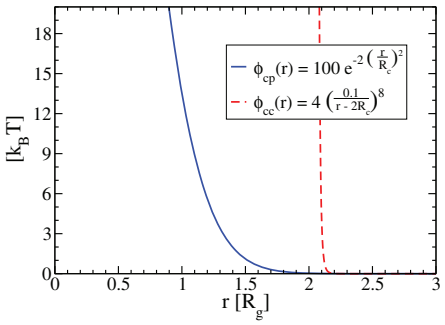

FIG. 6. The colloid-colloid (red) and colloid-polymer (blue) interaction potentials.

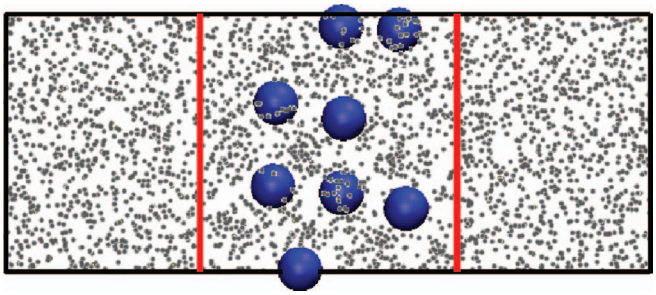

FIG. 7. Illustration of the simulation box used to find the equilibrium chain density in the system with colloids. The polymers (gray dots) can pass through the walls (red lines), while the colloids (blue spheres) are restrained to the region between the walls. The lateral dimension of the regions external to the walls is continuously adjusted by a density-based rescaling routine in order to achieve the desired bulk polymer density in the outer regions.

colloid-polymer interaction is based on the previous work by Bolhuis and Louis,[46] who inverted structural information from simulated sphere-polymer distribution functions. The exponential form of the potential allows the center of mass of a polymer or micellar chain to occasionally approach the center of the colloid to within less than $R_{\rm col}$. This softness represents the ability of long flexible chains to enlace a colloidal particle and thereby to locate its center of mass inside the colloid.

The motions of the colloids are described by a regular Brownian dynamics expression. The displacement of colloid i over a simulation time step dt is therefore similar in nature to Eq. (10). Since the colloids cannot entangle with the solvent chains, they are not subjected to entanglement forces and their friction coefficient is fixed at $\xi_i = \xi_c = 7 \cdot 10^{-7}$ kg/s. Under shear flow, the friction again acts relative to the prevailing flow field at the position of the colloid's center, resulting in the above discussed displacement contribution $+V(y_i)\hat{\mathbf{e}}_x dt$.

B. Preparation of colloidal dispersions

The colloid-polymer potential described in Fig. 6 does not allow any conclusion about the volumes occupied by the colloids and excluded to the polymers. We, therefore, do not know how many polymers should be removed with every colloid dispersed in the liquid. In order to calculate this number, we first ran a simulation with polymers all over the box and the colloids restricted to a central region measuring about one-third of the total box volume. The colloids were kept in this dispersion of volume $V_{\rm disp}$ by means of two semi-permeable walls, as depicted in Fig. 7, that were impermeable to the colloids but permeable to the polymers. The lateral box dimensions were gradually adjusted by a barostat-like algorithm, at fixed positions of the semi-permeable walls, to allow the polymer density in the two outer regions to equilibrate to the experimental polymer density $\rho_{\rm exp}$. As a result, the polymer chemical potential throughout the entire box became equal to its experimental value. The resulting number of polymers in the dispersion is by definition equal to

$$N_p^{\rm disp} = \rho_{\rm exp}(V_{\rm disp} - N_{\rm col} v_{\rm app}), \tag{19}$$

where N_c is the number of colloids and $v_{\rm app}$ is the apparent volume occupied by one colloid. From the simulation, we found $v_{\rm app} \approx -0.2R_g^3$. This volume value is rather different from the poorly defined volume of $\sim\frac{4}{3}\pi R_c^3$ of a colloid with soft interaction potentials; the small negative value even implies that the dispersion contains slightly more polymers than an equal volume of polymer fluid at the same chemical potential. The low apparent volume indicates that osmotic pressure of the polymer bath pushes the polymers against the colloids and thereby increases their overall density. The radial distribution function of polymers relative to colloids shows a peak at a distance of 1.6 R_g, indicating that the polymers are condensing against the colloids. Since the polymer-colloid interaction is purely repulsive, this condensation emerges as a consequence of the inter-polymer Flory-Huggins free energy. We inserted the value for $v_{\rm app}$ into Eq. (19) to calculate the appropriate number of polymers for the various colloidal suspensions of Secs. IV C–IV D. This procedure enabled us to find the correct density in the colloid-polymer system. Since the apparent volume of the colloid is a thermodynamic property of the interaction potentials, the aforementioned value obtained for the polymer solution also applies to colloids dispersed in worm-like micellar solutions. For completeness, we note that the colloidal ordering discussed below does not prove sensitive to the polymer density at the prevailing conditions, as very similar results were obtained upon equating $v_{\rm app}$ to $\frac{4}{3}\pi R_c^3$.

An important observation from the non-sheared simulations is that the colloids remain homogeneously distributed throughout the suspending fluid. The colloid-colloid radial distribution function (not shown) shows a first peak just beyond the colloidal diameter of 2 R_c, as is usual with hard sphere systems at intermediate or high densities.

C. Colloids in sheared micellar solutions

The behavior of colloids under shear was first simulated for the solution of worm-like micelles, since this fluid is known from experiments to induce colloidal alignment in the bulk.[6] In this and all subsequent simulations, the colloids were immersed in a rectangular simulation box measuring $24 \times 16 \times 12R_g^3$. To facilitate the formation of colloidal strings, in the expectation that they would occur, the 30 colloids of the initial box were placed in a plane spanned by the shear velocity and the velocity-gradient, i.e., the xy-plane, taking care to prevent any significant overlap while randomly

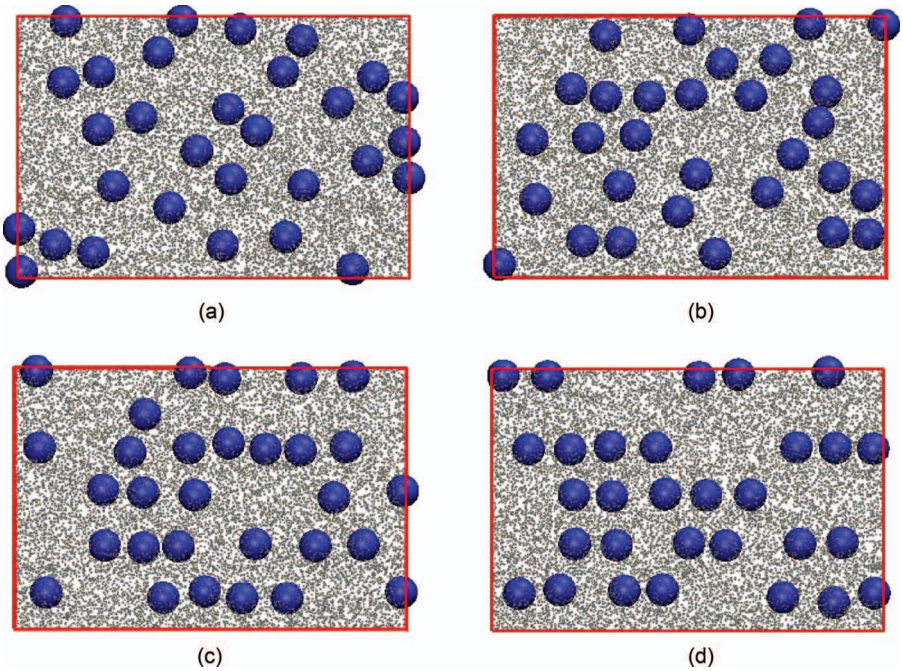

FIG. 8. Snapshots of 30 colloids (blue spheres, volume fraction $\varphi = \frac{4}{3}\pi N_{\rm col} R_{\rm col}^3 / V_{\rm box} = 3\%$), initially distributed over the xy-plane, with the shear flow along the horizontal x-direction and the velocity-gradient along the vertical y-direction. The pictures show projections on the xy-plane at (a) $t = 0$ s, (b) $t = 0.1$ s, (c) $t = 2$ s, and (d) $t = 4$ s after the onset of a $\dot\gamma = 15\ {\rm s}^{-1}$ shear in a 3D worm-like micellar solution (gray dots). Side views of this system after 0 and 20 s are included in Fig. 9.

placing the colloids. The procedure outlined in Sec. IV B was used to calculate the number of fluid particles filling the remaining unoccupied volume of the box. A strong shear flow of $\dot\gamma = 15\ {\rm s}^{-1}$, well beyond the transition to shear-thinning in Fig. 5, was imposed on the system. In order to reduce the usual complicating start-up effects at the onset of shear flow, the simulation was started at $t = 0$ with the expected steady state linear fluid velocity $V(y) = \dot\gamma\, y \hat{\mathbf{e}}_x$, and then left to evolve freely. Snapshots from the simulation at various times are shown in Fig. 8. The first frame shows the initial box, with the colloids distributed randomly in the xy-plane. The second and third frames, taken at 0.1 s and 2 s, respectively, clearly show a gradually increasing degree of ordering. In the last snapshot, taken after 4 s, the particles have converged to form strings along five parallel lines in the flow direction; this set of five lines survived for the next 16 seconds, at which point the simulation was terminated. Watching movies of this and similar systems revealed that the colloidal strings are anything but stationary. Besides the obvious convective motion along the shear direction, the strings repeatedly lose one or two colloids from their tails, which subsequently are caught by and become the head of the next string moving along the same flow line. The microscopy image in Fig. 2(a) of Ref. 6 suggests similar behavior under experimental conditions, as the photographed strings of colloids resemble trains running along the same track. The order of the colloids along the flow line typically stays the same, though we have seen occasions where a colloid briefly left a string and was overtaken by (part of) the string before returning to the flow line. The five lines also performed erratic Brownian motions, thus changing their vertical spacing and gradually drifting away from the initial $z = 0$ plane.

To quantify the degree of colloidal alignment, the area covered by the colloids in a projection onto the yz-plane was computed as a function of time. Figure 9 shows how this covered area initially decreased rapidly, reached a plateau after around 3 s, and remained essentially constant from this time onward. The inset displays snapshots at the beginning and end of the simulation, which clearly show that the system evolved from a disordered to an ordered configuration. Note that one colloid, near the bottom of the second snapshot, has escaped from the xy-plane to wander around on its own.

One may object that the above ordering could be a consequence of our starting with all colloids confined to a single

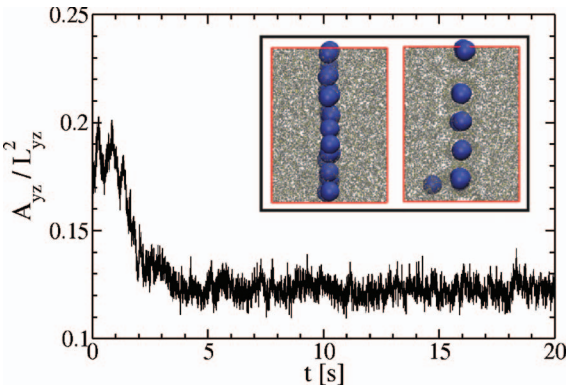

FIG. 9. The fraction of the yz-plane covered by colloids, as a function of time, in a worm-like micellar solution sheared at $\dot\gamma = 15\ {\rm s}^{-1}$. The 30 colloids were initially randomly distributed over the xy-plane, as shown in the left inset. At the end of the 20 s run, the colloids were arranged into five lines, as is clearly visible in the right inset. Note how one colloid near the bottom of the box has escaped the xy-plane. Four snapshots showing front views of the aligning process are shown in Fig. 8.

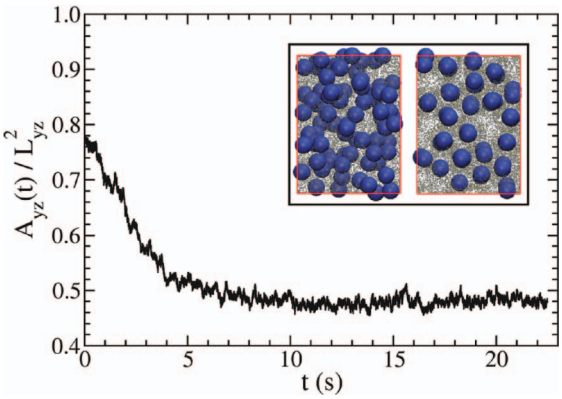

FIG. 10. Fractional area of the yz-plane occupied by 80 colloids, $\varphi = 7\%$, as an initially dispersion in a worm-like micellar solution gradually orders under a simple shear flow of $\dot{\gamma} = 15\ s^{-1}$. The inset displays snapshots in the yz-plane of the initial (left) and final (right) configurations.

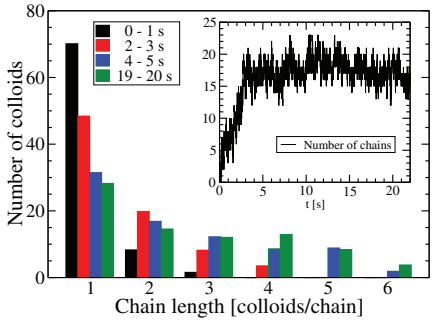

FIG. 11. Histogram of the number of colloids in chains of given lengths, averaged over four intervals of 1 s, for initially homogeneous suspension of 80 colloids, in a worm-like micellar solution sheared at $\dot{\gamma} = 15\ s^{-1}$. The sum area of all bars at any given time equals the total number of colloids in the system. The inset shows the number of colloidal string as a function of time. See the main text for the operational definition of a string. Only strings of two or more colloids are counted.

plane. We therefore also performed simulations on a system containing 80 colloids which were initially placed randomly throughout the entire box, again taking care to avoid overlap when generating the configuration. Figure 10 shows the evolution, at a shear rate of $\dot{\gamma} = 15\ s^{-1}$, of the yz area occupied by the colloids as a function of time. The high initial coverage of nearly 80% rapidly decreases over the course of about 7 s to a stable level of just under 50%. This decrease is also evident from the snapshots, shown as insets to the figure, of the initial and final configurations of the 22 s long simulation. Interestingly, the final configuration suggests that the strings of colloids adopt an hexagonal ordering in the yz-plane.

A second method to quantify the alignment of the colloids is to count the number of colloidal strings and their lengths. For particles i and j to qualify as neighboring members of the same colloidal string, the difference vector $\mathbf{r}_{ij}$ between their centers had to be limited (i) in the flow direction to $|r_{ij,x}| \leq 3R_g$, and (ii) in the perpendicular direction by $r_{ij,y}^2 + r_{ij,z}^2 \leq (0.5R_g)^2$. A simple algorithm then grouped all neighbor-linked colloids together to identify all strings of at least two colloids. The inset in Fig. 11 shows that, under shear, the 80 randomly distributed colloids grouped into a steadily growing number of strings, which after about 4 s reached a steady value at about 18 strings. Of course, the precise number of colloidal strings varies with the definition of neighbors, but the overall result clearly confirms the shear-alignment implied by the reduction of the projected yz-area. Figure 11 also shows the distribution of colloids over the various string lengths, at several intervals during the simulation. The approximate 70 colloids in "strings" of one colloid over the first second of the simulation confirms that the colloids are initially randomly distributed. At the intermediate times from 2 s to 3 s and from 4 s to 5 s, the number of free colloids decreases as ever more and longer strings are being formed. The average number of free colloids at the end of the simulation, from 19 s to 20 s, has reduced by five more colloids, but the most notable change is the growth of the long chains.

The dominant center-to-center distance between colloids in these strings, as derived from the first peak in the in-line distance distribution (not shown), lies at about 2.4 R_g. Hence, the colloids hardly touch each other, as their interaction energy is virtually zero at this separation, while at the same time the space between consecutive colloids is too narrow to accommodate fluid particles, as was confirmed by examining movies of the system. The latter suggests that depletion interactions may be contributing to the stability of shear-induced colloidal strings, though we recall that our earlier observations showed that the depletion interactions at zero shear are too weak to induce alignment. Combining the average spacing with the box dimensions, we note that the longest possible chain is expected to contain 10 colloids, well beyond the longest string observed in our simulations.

The evolutions of the shear stresses S_{xy} in the pure fluid and the suspension are plotted in Fig. 12. Since the simulations were started with the expected linear steady state velocity profile, the shear stress in the pure fluid almost immediately reaches its steady state value. The shear stress of the colloidal suspension initially decays fast, but after ~5 s only a very slow decrease remains which appears to converge to a steady level. This transition time roughly coincides with the time it takes for the randomly distributed colloids to aggregate into strings, as follows by a comparison of Figs. 10 and 12, which in combination with the absence of start-up effects in the pure fluid suggests that colloidal alignment reduces the shear stress. The alignment proceeds faster than under experimental conditions because we have stepped over the slow evolution from a quiescent fluid to a steady sheared state, because the colloidal concentration is higher by about one order of magnitude, and possibly also benefits from the enhanced Brownian motions of the smaller colloids. Since the rate of energy dissipation by the sheared fluid is given by $P = S_{xy}\dot{\gamma} L_z$, the decreasing shear stress may be re-interpreted as an evolution of the colloidal suspension towards a steady state requiring minimum power dissipation. Interestingly, we observed similar relaxations to steady states of minimum dissipation in several system that we studied recently, including shear-banding of a viscoelastic fluid in the RaPiD simulations[27,40] and segregation of granules in a rotating drum,[47] which tentatively suggests that a reduction of the dissipation rate may act as a driving mechanism inducing ordering in driven systems. For an extensive discussion on possible generic physical laws governing non-equilibrium

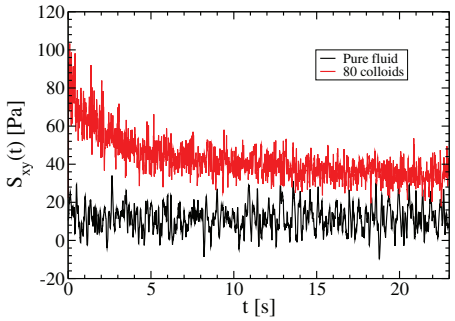

FIG. 12. The shear stress S_{xy} against the time for a worm-like micellar solution containing 80 initially randomly distributed colloids (red), at a constant shear rate of $\dot{\gamma} = 15\ s^{-1}$, and for the pure fluid (black). The former has a higher viscosity because of the suspended colloids, as well as due to the higher micellar concentration dictated by the constant chemical potential (see Section IV B).

steady states, and the evolution toward these states, we refer the reader to the review of Martyushev and Seleznev[48] and the book by Öttinger.[49]

In our simulations, a sufficiently high shear rate proved crucial to the shear-induced alignment of colloidal particles, as we did not observe any spontaneous alignment at shear rates below 3 s^{-1}. At these low shear rates, it is conceivable that the time scale of string formation exceeds the simulation time scale of about 20 s. We, therefore, investigated the stability of pre-assembled chains of colloids at these low shear rates. Figure 13 shows the projected area A_{yz} against the time for simulation boxes prepared with 12 strings of 8 colloids each, at an inter-colloid spacing of 2.4 R_g. The area increases approximately linearly in time for shear rates of 1 s^{-1} and below, including a non-sheared system, and thereby indicates that the colloids gradually disordered at these low shear rates. At $\dot{\gamma} = 2\ s^{-1}$, the area initially increased but then decreased again to settle at a somewhat "undecided" level. For $\dot{\gamma} \geq 3\ s^{-1}$, the projected area fluctuated around a constant value, slightly higher than the area of the perfectly aligned initial system, indicating that the alignment is stable at these high shear rates. These observations are in agreement with experimental observations of a critical shear rate of about 1 s^{-1} for large colloidal particles dispersed in the bulk worm-like micellar solution modeled here.[6] In all simulations of the micellar fluid, with and without colloids, the velocity profile

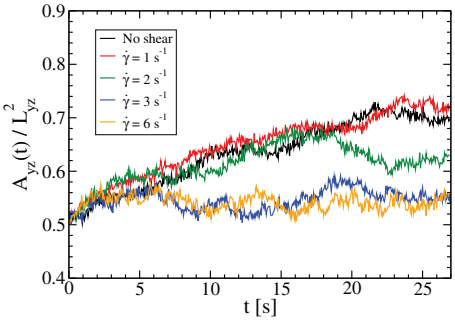

FIG. 13. Projected area A_{xy} occupied by 96 colloids, $\varphi = 9\%$, in worm-like micellar solutions at various shear rates. All simulations started from a perfectly aligned configuration with 12 strings of 8 colloids each.

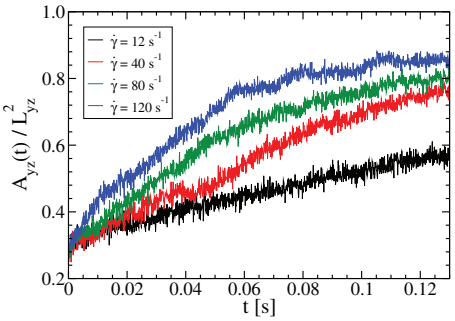

FIG. 14. The occupied projection area in the yz-plane by 96 colloids, initially forming 12 flow-aligned strings, dispersed in polymer solutions at various shear rates.

$V(y)$ of the flowing fluid was virtually linear, indicating that colloidal alignment does not require shear banding. This observation is also in agreement with experiments,[6] which indicate that shear-banding can promote alignment but is not a prerequisite.

D. Colloids in sheared polymer solutions

The preceding study on colloids in a worm-like micellar solution was repeated for colloids dispersed in the polymer solution. Following the same procedures, we first placed 30 colloids randomly in the xy-plane and applied a shear flow of $\dot{\gamma} = 15\ s^{-1}$ in the x-direction. This time, however, the colloids remained homogeneously distributed. We increased the shear rate stepwise in a set of simulations, but even at the highest shear rate of $\dot{\gamma} = 200\ s^{-1}$ the colloids still did not align. Next, we distributed 80 colloids randomly throughout the entire box and ran simulations over the same range of shear rates. Again, the particles remained randomly distributed at all applied shear rates up to $\dot{\gamma} = 200\ s^{-1}$.

To rule out low diffusivity as a possible cause for the absence of colloidal chains in the polymer solution, we also performed simulations on initial configurations of 96 colloids forming 12 straight lines along the flow direction. The projected area covered by these colloids gradually increased, see Fig. 14, indicating that the colloids were diffusing away from their initial ordered state to a disordered state. In fact, the misalignment proceeded quicker at higher shear rates, probably because of shear thinning. From this we learn that, even though the polymer solution behaves as a shear thinning viscoelastic fluid with a thinning-exponent of nearly -1, no ordering of particles is to be expected. This observation agrees with the experimental observation that colloids in this polymeric fluid do not align in the bulk (but migrate to the rheometer walls and align there),[8,50] and confirms that bulk alignment is limited to a subset of shear-thinning fluids. In contrast to the worm-like-suspension, the shear stress and hence the power dissipation in the polymeric suspension reach their steady state values already after 0.05 s.

V. CONCLUSIONS

We have performed coarse-grained simulations of colloidal particles dispersed in two viscoelastic fluids with

rheological behaviors typical of semi-dilute solutions containing polymers and worm-like micelles, respectively, at a volume fraction of 11% or nearly 15 times the critical overlap concentration. Each polymeric or micellar chain was represented by a single particle in RaPiD, enabling simulations covering large length and time scales; in this study, a standard desktop processor sufficed to simulate fluid volumes of 0.3 μm^3 for 20 s. In order to recover the rheological behavior of the fluids, the particles were endowed with configuration and time-dependent memory effects which qualitatively describe the entanglement effects responsible for the dynamics of the real chains. This study shows that markedly different rheological behaviours of two shear-thinning fluids are well reproduced quantitatively by RaPiD simulations, through the adjustment of a few simulation parameters. For convenience, we endowed here both fluids with identical thermodynamic properties, to specifically concentrate on the impact of fluid rheology on the ordering of suspended colloids in sheared bulk suspensions. The simulations showed that the colloids formed strings along the shear direction in the worm-like micellar solution, provided the shear rate exceeded 2 s^{-1}, while the colloids in the polymeric solution remained homogeneously dispersed throughout the bulk at all shear rates. These results are in good agreement with recent experimental studies in the group of Vermant on colloids dispersed in the two fluids modeled here, reporting alignment in the bulk worm-like solution beyond 1 s^{-1} and disorder in the bulk of the polymeric solution.[6,8,50]

The simulations indicate that the shear-aligned colloids are nearly touching, leaving insufficient space for worm-like micelles to reside between consecutive colloids. While this suggests that depletion interactions are involved in the colloidal alignment, we note that depletion interactions were not capable of inducing aggregation at low and vanishing shear rates, nor can these thermodynamic attraction forces explain the marked difference in colloidal aggregation between micellar and polymeric solutions (since the simulated fluids share thermodynamic behavior). These results are supported by experiments, with the colloids nearly touching under shear in the micellar solution but randomly dispersed at low shear rates in both solutions.[6,50] Hence, we are led to speculate that the depletion forces are secondary to a still unidentified flow-induced driving force, which in the bulk micellar solution is sufficiently strong to overcome Brownian motion but in the bulk polymer solution is weak or absent. An interesting observation in this respect is the decreasing power dissipation by the dispersion concomitant with increasing colloidal alignment, which might place this ordering phenomenon within the wider—yet still incompletely understood—context of dissipative non-equilibrium steady states.[48,49]

An important difference between the simulation approach advocated here and the approaches taken by most authors studying colloids in viscoelastic fluids[13,20,21,51] is that we do not employ a numerical Navier-Stokes solver to explicitly calculate the flow field throughout the entire simulation box. The RaPiD approach drastically reduces the computational burden, thereby enabling RaPiD to simulate larger systems with more colloids and in full three-dimensional space.

We express the hope that additional studies with the RaPiD method, by systematically exploring the effects of the fluid parameters, will help elucidate the intriguing mechanism behind shear-induced alignment in the bulk as well as at the walls.

ACKNOWLEDGMENTS

The authors thank the financial support of the European Commission through the seventh framework program, project Nanodirect NMP4-SL-2008-213948, the EU Network of Excellence SoftComp for access to the Jülich supercomputing center, and Professor Jan Vermant for providing experimental data.

APPENDIX: FLORY-HUGGINS FREE ENERGY FOR A SYSTEM OF CHAINS WITH FIXED CENTRAL SEGMENT

In this Appendix we present the potential of mean force that we have used in our simulations. Out of all degrees of freedom in our system we only keep track of the central monomer of each polymer. The potential of mean force, therefore, is the free energy of all polymers for given position of their central monomers. We will calculate this free energy using a Landau-de Gennes type of description of inhomogeneous systems.

Consider a very large box of volume V containing N_s solvent molecules and N_p polymers each consisting of p Kuhn lengths. According to the incompressible Flory-Huggins model the total free energy A may be calculated according to

$$A = -kT \ln Q_{N_s,N_p}, \tag{A1}$$

$$Q_{N_s,N_p} = \left(\frac{q_s^{int}}{\Lambda_s^3}\right)^{N_s} \left(\frac{q_p^{int}}{\Lambda_p^3}\right)^{pN_p} \left(\frac{z-1}{M}\right)^{N_p(p-1)} \times \frac{M!}{N_s!N_p!} \exp(-\beta U)\Delta^{N_s+pN_p}, \tag{A2}$$

where $M = V/\Delta$ is the number of cubes of size Δ into which the total volume has been divided and z is the coordination number of the lattice that has been used. Furthermore, q_s^{int} and q_p^{int} are single particle partition functions accounting for internal degrees of freedom in each lattice cell, and Λ_s and Λ_p are the corresponding thermal de Broglie wavelengths. Finally, U is the average interaction energy

$$U = \frac{1}{2}z\left\{\frac{N_s^2}{M}(-\epsilon_{ss}) + 2p\frac{N_sN_p}{M}(-\epsilon_{sp}) + p^2\frac{N_p^2}{M}(-\epsilon_{pp})\right\}, \tag{A3}$$

where ϵ_{ij} are interaction energies between neighboring cubes of species i and j. On average the central segments of the polymers will be homogeneously distributed throughout the box. Thermal fluctuations around this homogeneous distribution must be sampled correctly by our simulations. In order to

achieve this we must calculate the relative probabilities, i.e., the relative free energies of such fluctuations. First notice that if we reshuffle the central segments in order to generate a fluctuation, the number of solvent molecules and the number of polymers do not change. We may, therefore, eliminate all contributions to the free energies which are linear in the number of solvent molecules or the number of polymers from further considerations. We are then left with

$$A' = kTN_p \ln\left(\frac{N_p}{M}\right) + kTN_s \ln\left(\frac{N_s}{M}\right) - \frac{p^2 N_p^2}{M}\chi, \tag{A4}$$

$$\chi = \frac{1}{2}\beta z(\epsilon_{ss} + \epsilon_{pp} - 2\epsilon_{sp}), \tag{A5}$$

where χ is the Flory-Huggins parameter. Next, we notice that the simulated degrees of freedom take care of

$$A^{sim} = -kT \ln\left(\frac{V^{N_p}}{N_p!}\right). \tag{A6}$$

The free energy of the eliminated degrees of freedom may therefore be taken to be $A' - A^{sim}$, which on neglecting the terms proportional to N_p leads to

$$A'' = kTpN_p\left\{\frac{1-\phi}{\phi}\ln(1-\phi) - \chi\phi\right\}, \tag{A7}$$

where we have introduced the volume fraction

$$\phi = p\frac{N_p}{M}. \tag{A8}$$

In order to discriminate the various inhomogeneous distributions of the central segments from one another, we have introduced local densities $\phi_i(r)$ around each particle i. We now assume that the corresponding (relative) free energies may be approximated as

$$\Phi_C(r) = kTp \times \sum_{i=1}^{N_p}\left\{\frac{1-\phi_i(r)}{\phi_i(r)}\ln(1-\phi_i(r)) - \chi\phi_i(r)\right\}, \tag{A9}$$

$$= \sum_{i=1}^{N_p} kTa^p(\phi_i(r)), \tag{A10}$$

where the second line serves to define $a^p(\phi_i(r))$.

The force acting on each particle can now be expressed in terms of the local volume fraction as

$$\mathbf{F}_i = -\nabla_i A[\rho] = -\nabla_i \sum_{j=1}^{N} a^p(\phi_j) = -\sum_{j=1}^{N}\frac{da^p(\phi_j)}{d\phi_j}\frac{\partial\phi_j}{\partial\rho_j}\frac{\partial\rho_j}{\partial\mathbf{r}_i}, \tag{A11}$$

which results in a quasi-pairwise interaction (quasi because the local density does depend on the location of other particles),

$$\mathbf{F}_i = -\frac{1}{\rho_{max}}\sum_{j=i}^{N}\left(\frac{da^p(\phi_j)}{d\phi_j} + \frac{da^p(\phi_i)}{d\phi_i}\right)\frac{\partial}{\partial\mathbf{r}_i}\omega(r_{ij}). \tag{A12}$$

[1] R. G. Larson, *The Structure and Rheology of Complex Fluids* (Oxford University Press, Oxford, U. K., 1999).
[2] J. Michele, R. Patzold, and R. Donis, Rheol. Acta **16**, 317 (1977).
[3] M. K. Lyon, D. W. Mead, R. E. Elliott, and L. G. Leal, J. Rheol. **45**, 881 (2001).
[4] R. Scirocco, J. Vermant, and J. Mewis, J. Non-Newtonian Fluid Mech. **117**, 183 (2004).
[5] D. Won and C. Kim, J. Non-Newtonian Fluid Mech. **117**, 141 (2004).
[6] R. Pasquino, F. Snijkers, N. Grizzutti, and J. Vermant, Langmuir **26**, 3016 (2010).
[7] A. Y. Malkin, A. V. Semakov, and V. G. Kulichikhin, Adv. Colloid Interface Sci. **157**, 75 (2010).
[8] R. Pasquino, F. Snijkers, N. Grizzutti, and J. Vermant, Rheol. Acta **49**, 993 (2010).
[9] J. M. Manski, A. J. van der Goot, and R. M. Boom, Trends Food Sci. Technol. **18**, 546 (2007).
[10] J. Feng, P. Y. Huang, and D. D. Joseph, J. Non-Newtonian Fluid Mech. **63**, 63 (1996).
[11] H. Binous and R. J. Phillips, J. Non-Newtonian Fluid Mech. **83**, 93 (1999).
[12] O. G. Harlen, J. Non-Newtonian Fluid Mech. **108**, 411 (2002).
[13] Z. Yu, A. Wachs, and Y. Peysson, J. Non-Newtonian Fluid Mech. **136**, 126 (2006).
[14] A. M. Ardekani, R. H. Rangel, and D. D. Joseph, Phys. Fluids **20**, 063101 (2008).
[15] W. R. Hwang, M. A. Hulsen, and E. H. Meijer, J. Non-Newtonian Fluid Mech. **121**, 15 (2004).
[16] N. A. Patankar and H. H. Hu, J. Non-Newtonian Fluid Mech. **96**, 427 (2000).
[17] G. D'Avino, M. A. Hulsen, F. Snijkers, J. Vermant, F. Greco, and P. L. Maffetone, J. Rheol. **52**, 1331 (2008).
[18] G. D'Avino, G. Cicale, M. A. Hulsen, F. Greco, and P. L. Maffetone, J. Non-Newtonian Fluid Mech. **157**, 101 (2009).
[19] G. D'Avino, P. L. Maffetone, F. Greco, and M. A. Hulsen, J. Non-Newtonian Fluid Mech. **165**, 466 (2010).
[20] R. J. Phillips and L. Talini, J. Non-Newtonian Fluid Mech. **147**, 175 (2007).
[21] W. R. Hwang and M. A. Hulsen, Macromol. Mater. Eng. **296**, 321 (2011).
[22] A. van den Noort, W. K. den Otter, and W. J. Briels, Europhys. Lett. **80**, 28003 (2007).
[23] W. J. Briels, Soft Matter **5**, 4401 (2009).
[24] F. Snijkers, G. D'Avino, P. L. Maffetone, F. Greco, M. Hulsen, and J. Vermant, J. Rheol. **53**, 459 (2009).
[25] J. M. Deutch and I. Oppenheim, J. Chem. Phys. **54**, 3547 (1971).
[26] P. Mazur and I. Oppenheim, Physica **50**, 241 (1970).
[27] A. van den Noort and W. J. Briels, Macromol. Theory Simul. **16**, 742 (2007).
[28] P. Kindt and W. J. Briels, J. Chem. Phys. **127**, 134901 (2007).
[29] J. Sprakel, E. Spruijt, J. van der Gucht, J. T. Padding, and W. J. Briels, Soft Matter **5**, 4748 (2009).
[30] J. T. Padding, E. van Ruymbeke, D. Vlassopoulos, and W. J. Briels, Rheol. Acta **49**, 473 (2010).
[31] J. T. Padding, L. V. Mohite, D. Auhl, W. J. Briels, and C. Bailly, Soft Matter **7**, 5036 (2011).
[32] J. Sprakel, J. T. Padding, and W. J. Briels, Europhys. Lett. **93**, 58003 (2011).
[33] P. Kindt and W. J. Briels, J. Chem. Phys. **128**, 124901 (2008).
[34] P. J. Flory, J. Chem. Phys. **10**, 51 (1942).
[35] M. L. Huggins, J. Chem. Phys. **9**, 440 (1941).
[36] M. Doi and S. F. Edwards, *The Theory of Polymers Dynamics* (Oxford Science, Oxford, UK, 1986).
[37] R. L. C. Akkermans and W. J. Briels, J. Chem. Phys. **115**, 6210 (2001).
[38] M. P. Allen and D. J. Tildesley, *Computer Simulations of Liquids* (Oxford University Press, Oxford, London, 1987).
[39] J. T. Padding, E. S. Boek, and W. J. Briels, J. Chem. Phys. **129**, 074903 (2008).

[40]A. van den Noort and W. J. Briels, J. Non-Newtonian Fluid Mech. **152**, 148 (2008).
[41]M. E. Cates and S. J. Candau, J. Phys.: Condens. Matter **2**, 6869 (1990).
[42]L. M. Walker, Curr. Opin. Colloid Interface Sci. **6**, 451 (2001).
[43]S. Ezrahi, E. Tuval, and A. Aserin, Adv. Colloid Interface Sci. **128**, 77 (2007).
[44]C. A. Dreiss, Soft Matter **3**, 956 (2007).
[45]V. G. Mavrantzas, T. D. Boone, E. Zervopoulou, and D. N. Theodorou, Macromolecules **32**, 5072 (1999).
[46]P. G. Bolhuis and A. A. Louis, Macromolecules **35**, 1860 (2002).
[47]M. M. H. D. Arntz, W. K. den Otter, H. H. Beeftink, R. M. Boom, and W. J. Briels, Europhys. Lett. **92**, 54004 (2010).
[48]L. M. Martyushev and V. D. Seleznev, Phys. Rep. **426**, 1 (2006).
[49]H. C. Öttinger, *Beyond Equilibrium Thermodynamics* (Wiley-Interscience, Hoboken, NJ, 2005).
[50]J. Vermant, private communication (14 May 2011).
[51]G. D'Avino, T. Tuccillo, P. L. Maffetone, F. Greco, and M. A. Hulsen, Comput. Fluids **39**, 709 (2010).